Liquid Crystals
Publication details, including instructions for authors and subscription information:
http://www.informaworld.com/smpp/title~content=t713926090

Modelling of the simple shear flow of a flow-aligning nematic

Grzegorz Derfel; Barbara Radomska

Online publication date: 29 June 2010

To cite this Article Derfel, Grzegorz and Radomska, Barbara(1997) 'Modelling of the simple shear flow of a flow-aligning nematic', Liquid Crystals, 23: 5, 741 — 748
To link to this Article: DOI: 10.1080/026782997208019
URL: http://dx.doi.org/10.1080/026782997208019

LIQUID CRYSTALS, 1997, VOL. 23, NO. 5, 741–748

Modelling of the simple shear flow of a flow-aligning nematic

by GRZEGORZ DERFEL* and BARBARA RADOMSKA
Institute of Physics, Technical University of Łódź, ul. Wólczańska 223,
93-005 Łódź, Poland

(*Received 20 May 1996; in final form 14 June 1997; accepted 24 June 1997*)

The shear flow induced deformations of a nematic liquid crystal layer have been modelled numerically for the case of flow-aligning nematics. The director deviation from the plane of shear, which was predicted earlier for special surface orientation angles, has been confirmed. This deformation takes a form of director rotation about the axis perpendicular to the layer plane. As a result, transverse flow of the nematic arises. The rotation angle is close to π at sufficiently strong shear stress, and the director is oriented at the usual flow alignment angle in a significant part of the layer. The director coming out of the shear plane should not be treated as a separate effect taking place during the flow, but rather as a way in which the usual flow-aligned structure is achieved.

1. Introduction

The shear flow induced alignment of nematic liquid crystals, characterized by the viscosity coefficients ratio $\alpha_3/\alpha_2 > 0$, is a well known phenomenon [1]. Under the influence of the viscous torque, the director **n** forms an angle θ_c against the direction of flow

$$\theta_c = \arctan\left[(\alpha_3/\alpha_2)^{1/2}\right]. \qquad (1)$$

However, even in simple shear flow, the variety of possible effects is still not recognized comprehensively. The initial director orientation within the plane of shear, imposed by the boundary interactions, was found to be crucial for shear flow induced deformations [2–4]. In refs [2] and [3], director configurations confined to the shear plane were assumed. Two distinct types of deformations were found. They were characterized by high shear stress induced alignment angles equal to θ_c and $\theta_c - \pi$, respectively. The former structure was realized if the boundary orientation angle θ_s varied in the range $(\pi/2, -\theta_c)$. The latter configuration took place if $\theta_s \in (-\theta_c, -\pi/2)$, and was related with much larger elastic energy. The elastic deformation was especially strong if θ_s was slightly smaller than $-\theta_c$. However, as was shown qualitatively in ref. [4], the flow alignment effect has a different character, since the director may come out of the plane of shear, but only if the shear stress exceeds a certain threshold value. Coming out of the shear plane should occur if θ_s takes a value from some range contained in $(-\theta_c, -\pi/2)$.

In the present work, we studied the shear flow alignment effect quantitatively by means of numerical simulation. We have found that the director rotates about the axis perpendicular to the layer plane. This rotation generates the usual flow-aligned structure, which prevails in the layer at sufficiently high stress. Therefore, the director deviation from the shear plane should not be considered as a separate effect taking place during flow, but rather as a way in which the usual flow-aligned structure is achieved.

*Author for correspondence.

2. Method

The calculations were performed for an infinite layer with strong boundary anchoring. One-dimensional deformations were assumed. Director distributions in the sheared layer were calculated for various surface induced orientations and shear stresses.

The nematic liquid crystal was characterized by the elastic constant ratios $k_t = k_{22}/k_{11}$, $k_b = k_{33}/k_{11}$ and the viscosity coefficients ratios α_i/α_2, $i = 1 \ldots 6$. The flow-aligning nematic, i.e. the material with $\alpha_3/\alpha_2 > 0$, was considered. The material was confined in a layer of thickness d between two plates parallel to the xy plane and positioned at $z = \pm d/2$. The lower plane was at rest while the upper moved along the y axis under the action of a constant shear stress τ. The stationary director distribution in the deformed layer was described by two angles: the tilt angle, $\theta(z)$, between director and its projection n_{xy} on the xy plane, and by the deviation angle, $\phi(z)$, between n_{xy} and the y axis (figure 1). The angle $\theta(z)$ was a measure of the director deviation from the xy plane. The angle $\phi(z)$ stood for the director rotation about the z axis, and was a measure of the deviation from the shear plane yz. Boundary conditions were determined by rigid anchoring, identical at both

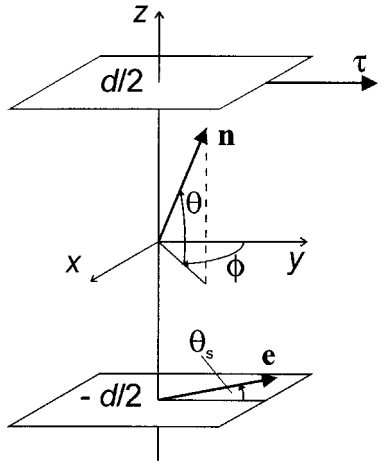

Figure 1. The geometry of the system.

plates. Surface director orientation was determined by the easy axis versor **e**, which lay in the yz plane and formed the angle θ_s against the y axis. The anchoring free energy per unit area of the layer was assumed in the Rapini–Papoular form

$$F_{\text{anchoring}} = -(W/2)(\mathbf{ne})^2 \tag{2}$$

where W is the anchoring strength coefficient.

In general, the stationary state in the sheared layer results from the balance of the elastic and viscous torques in the bulk, and the elastic, viscous and surface torques at the boundaries.

The elastic torque is

$$\Gamma_{\text{elastic}} = \mathbf{n} \times \mathbf{h} \tag{3}$$

where **h** is the molecular field. Its components are given by

$$h_j = \frac{\partial g_{\text{elastic}}}{\partial n_j} - \frac{\partial}{\partial z}\frac{\partial g_{\text{elastic}}}{\partial n_{j,z}} \tag{4}$$

where g_{elastic} is the Frank elastic free energy density and $n_{j,z} = \partial n_j/\partial z$ and $j \equiv x, y, z$.

The viscous torque is expressed by the viscous force $\mathbf{f}'$:

$$\Gamma_{\text{viscous}} = \mathbf{n} \times \mathbf{f}'. \tag{5}$$

The components of $\mathbf{f}'$ are

$$\begin{aligned} f'_x &= \alpha_2 w n_z \\ f'_y &= \alpha_2 u n_z \\ f'_z &= \alpha_3 (u n_y + w n_x) \end{aligned} \tag{6}$$

where $u = \partial v_y/\partial z$ and $w = \partial v_x/\partial z$. The velocity gradients u and w are given by the Navier–Stokes equations

$$\begin{aligned} \tau &= uP + wQ \\ \sigma &= uQ + wR \end{aligned} \tag{7}$$

where

$$P = \frac{1}{2}[2\alpha_1 n_y^2 n_z^2 + (\alpha_5 - \alpha_2) n_z^2 + (\alpha_3 + \alpha_6) n_y^2 + \alpha_4] \tag{8}$$

$$Q = \frac{1}{2}[2\alpha_1 n_x n_y n_z^2 + (\alpha_3 + \alpha_6) n_x n_y] \tag{9}$$

$$R = \frac{1}{2}[2\alpha_1 n_x^2 n_z^2 + (\alpha_5 - \alpha_2) n_z^2 + (\alpha_3 + \alpha_6) n_x^2 + \alpha_4] \tag{10}$$

and σ is the transverse shear stress appearing if the director deviates from the shear plane, i.e. if $n_x \neq 0$ or $\phi \neq 0$. The value of σ is determined by the 'no-slip condition'

$$\int_{-d/2}^{d/2} w \, dz = 0 \tag{11}$$

which leads to

$$\sigma = \tau \frac{\int_{-d/2}^{d/2} \frac{Q}{\Delta} dz}{\int_{-d/2}^{d/2} \frac{P}{\Delta} dz} \tag{12}$$

where $\Delta = PR - Q^2$.

The surface torque is expressed by

$$\Gamma_{\text{anchoring}} = W(\mathbf{n}\ \mathbf{e})(\mathbf{n} \times \mathbf{e}). \tag{13}$$

In our computer model, the continuous $\theta(z)$ and $\phi(z)$ functions were represented by a set of discrete values θ^i and ϕ^i determined in N equidistant planes positioned at $z^i = -d/2 + (i-1)d/(N-1)$, where $i = 1 \ldots N$. Each pair (θ^i, ϕ^i) was assigned to a sub-layer attached to each of the N planes. There were N sub-layers (figure 2). Two of them, of thickness $d/[2(N-1)]$, were adjacent to the boundary plates, and the remaining $N-2$ sub-layers, of thickness $d/(N-1)$, were placed in the bulk. The values θ^i and ϕ^i were used for calculation of the torques per unit volume which affected the director in the ith sub-layer. For each of the inner sub-layers, the sum of the elastic and viscous torques, given by equations (3) and (5) was calculated, while for the boundary sub-layers, the third torque due to the surface anchoring [equation (13)], was added.

The initial values of the angles were set to zero, whereas the initial angles ϕ^i were determined by the formula $\phi^i = \phi_0 \sin[\pi(i-1)/(N-1)]$, where ϕ_0 close to $\pi/2$ was chosen. The final set of angles, which approximated to the real stationary director distribution due to the equilibrium state, was calculated in the course of an

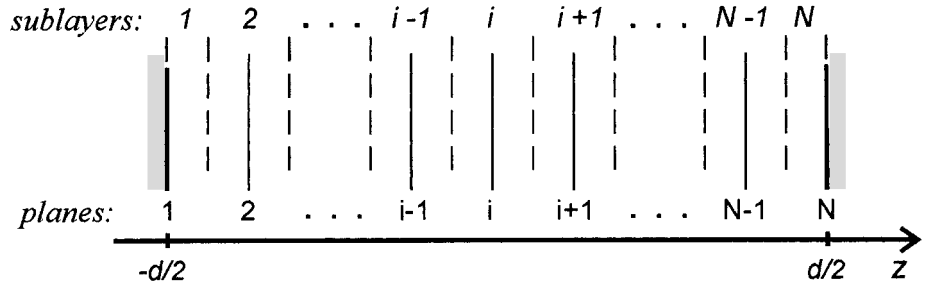

Figure 2. Planes and sub-layers distinguished within the layer.

iteration process. The values θ^i and ϕ^i were varied sequentially. The new values were accepted if they gave a small absolute value $|\Gamma^i|$ of the torque per unit volume in the ith sub-layer. This procedure was repeated until the sum of all $|\Gamma^i|$ decreased below some sufficiently low value ε in terms of the required accuracy. [In our calculations $\varepsilon = 10^{-4}$ while $N = 64$ gave a satisfactory approximation of the continuous $\theta(z)$ and $\phi(z)$ functions.] The set of angles obtained in this way for some value of the shear stress served as a starting point to computations of another shear stress value.

Some details concerning the use of the formulae mentioned above are given in the Appendix.

The director distribution allowed calculation of the effective viscosity coefficient

$$\eta = \frac{\tau d}{\int_{-d/2}^{d/2} \frac{\tau R - \sigma Q}{\Delta} \mathrm{d}z} \tag{14}$$

and the velocity components

$$v_x(z) = \int_{-d/2}^{z} \frac{\sigma P - \tau Q}{\Delta} \mathrm{d}z \tag{15}$$

$$v_y(z) = \int_{-d/2}^{z} \frac{\tau R - \sigma Q}{\Delta} \mathrm{d}z. \tag{16}$$

The integrations in the above expressions were performed numerically by use of the values θ^i and ϕ^i.

3. Results

The flow-aligning nematic with $\alpha_3/\alpha_2 = 0{\cdot}01$ was considered. The other material constants were: $k_b = 1{\cdot}2$, $k_t = 0{\cdot}4$, $\alpha_1/\alpha_2 = -0{\cdot}08$, $\alpha_4/\alpha_2 = -0{\cdot}62$, $\alpha_5/\alpha_2 = -0{\cdot}80$ and $\alpha_6/\alpha_2 = -0{\cdot}21$. The dimensionless parameter $\gamma = W d/k_{11}$, describing the anchoring strength, was equal to 2×10^5. The computations were carried out for five surface orientations: planar, homeotropic and three oblique, with the surface orientation angles $\theta_s = 0$, $\theta_s = \pi/2$, $\theta_s = -0{\cdot}3$, $\theta_s = -0{\cdot}11$ and $\theta_s = -0{\cdot}095$ rad, respectively. The two latter values are close to the critical angle $-\theta_c$, which takes the value $\theta_c = 0{\cdot}0997$ rad. For each case, the director distributions described by the functions $\theta(z)$ and $\phi(z)$, the transverse shear stress σ, the effective viscosity η, and the longitudinal and transverse velocity profiles $v_y(z)$ and $v_x(z)$ were determined for various values of the longitudinal shear stress τ. The functions $\theta(z)$ and $\phi(z)$ were always even, due to the symmetry of the problem, whereas the transverse velocity distribution functions $v_x(z)$ were odd. In the following, the results are presented in dimensionless form, obtained by means of suitable choice of units, i.e. d as the unit for distance, α_2 for viscosity, $k_{33}\pi^2/\alpha_2 d$ for velocity and $k_{33}\pi^2/d^2$ for stress.

3.1. *Planar and homeotropic layers*

In both cases, the director orientations at any stress are limited to the plane of shear. The mid-plane angles θ_m tend to θ_c, with increasing shear stress. The results are present in figure 3, where the profiles $\theta(z)$ are plotted for various dimensionless stress $t = \tau d^2/\pi^2 k_{33}$, and in figure 4, where the θ_m angles are plotted as functions of t. The effective viscosities vary smoothly with increasing t (figure 5).

3.2. *Oblique orientations*

The most interesting effects are expected for θ_s close to $-\theta_c$ [4], since the value $-\theta_c$ separates two ranges

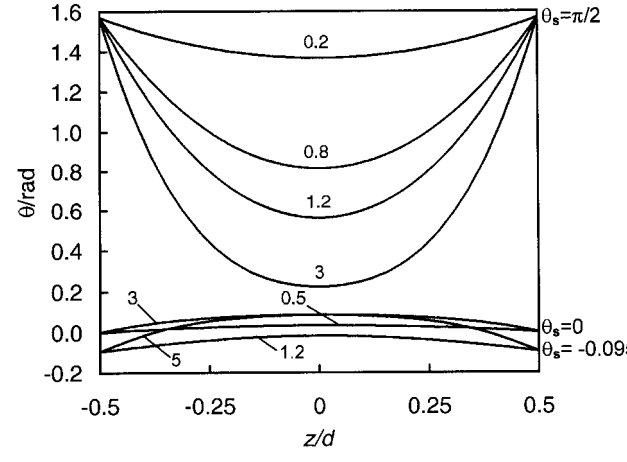

Figure 3. Director distribution $\theta(z)$ plotted for various shear stresses t in the homeotropic ($\theta_s = \pi/2$), planar ($\theta_s = 0$), and oblique ($\theta_s = 0{\cdot}095$) layers.

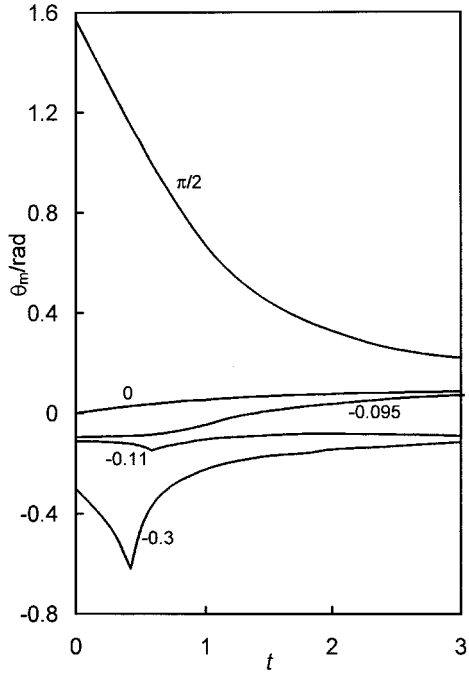

Figure 4. Mid-plane orientation angles θ_m as functions of shear stress t for five surface orientations $\theta_s\pi/2$, 0, $-0{\cdot}095$, $-0{\cdot}11$ and $-0{\cdot}3$ rad.

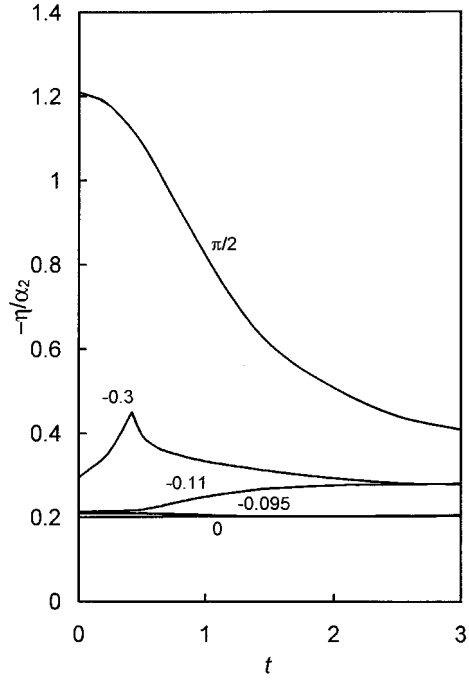

Figure 5. Effective viscosities η as functions of shear stress t for five surface orientations. (The curves for $\theta_s = 0$ and $\theta_s = -0{\cdot}095$ rad coincide approximately.)

of surface orientation angles, for which two different modes of deformation develop. The angle $\theta_s = 0{\cdot}11$ rad, which is slightly smaller than $-\theta_c$, is the first example. In this case two regimes of the shear stress can be distinguished. At low t, the director does not deviate from the shear plane. Above certain threshold stress, the emergence from the shear plane appears, i.e. the director rotates about the z axis. Twist deformations, with opposite sense of twist in both halves of the layer, arise; the corresponding functions $\theta(z)$ and $\phi(z)$ are shown in figure 6. The deformation can be characterized by the mid-plane values of both angles. The threshold behaviour of the mid-plane rotation angle ϕ_m is presented in figure 7; two senses of rotation are possible. The angle θ_m is plotted in figure 4 as a function of t; the threshold is revealed by the cusp on the $\theta_m(t)$ curve. The structure of the layer is illustrated in figure 8 by means of cylinders symbolizing the director. At high stress, the director in the middle part of the layer tends to the flow induced orientation $\phi_m \to \pi$ and $\theta_m \to \theta_c$ (which is identical with $\theta_m \to \theta_c$, $\phi_m \to 0$, due to the macroscopic physical equivalence of the director vectors $\mathbf{n}$ and $-\mathbf{n}$). The twist deformation is concentrated in the thin layers adjacent to the boundaries. A distribution of this kind results in significant transverse stress σ, as illustrated in figure 9; two senses of director rotation give opposite directions of σ. The behaviour of the effective viscosity is shown in figure 5, where η is plotted as a function of the longitudinal stress t.

Similar behaviour was found for the somewhat more tilted surface orientation $\theta_s = -0{\cdot}3$. The results are presented in figures 4, 5, 7, 9 and 10. The director also comes out of the shear plane when the threshold stress is exceeded. The cusp on the $\theta_m(t)$ curve is very pronounced; the cusp on the $\eta(t)$ curve also marks the emergence from the shear plane. [A similar singularity on the $\eta(t)$ curve is present for $\theta_s = -0{\cdot}11$ rad, but is not visible in figure 5.]

The peculiar effects presented above do not occur when the surface orientation angle θ_s is slightly bigger than $-\theta_c$. For instance, if $\theta_s = -0{\cdot}095$, the director does not deviate from the shear plane; the structure of the layer varies smoothly with increasing t. The corresponding curves are presented in figures 3 and 4. The $\eta(t)$ dependence does not differ significantly from that obtained for $\theta_s = 0$ (figure 5).

3.3. *Velocity profiles*

For a shear stress τ lower than the threshold, the nematic liquid crystal flows along the y axis; above the threshold stress, transverse flow appears, due to the director deviation from the shear plane. Figure 11 shows several examples for $\theta_s = -0{\cdot}11$. Transverse velocity profiles for $\theta_s = -0{\cdot}3$ are shown in figure 12. The longitudinal velocity $v_y(z)$ increases monotonically with z, as exemplified in figure 13 for the same surface align-

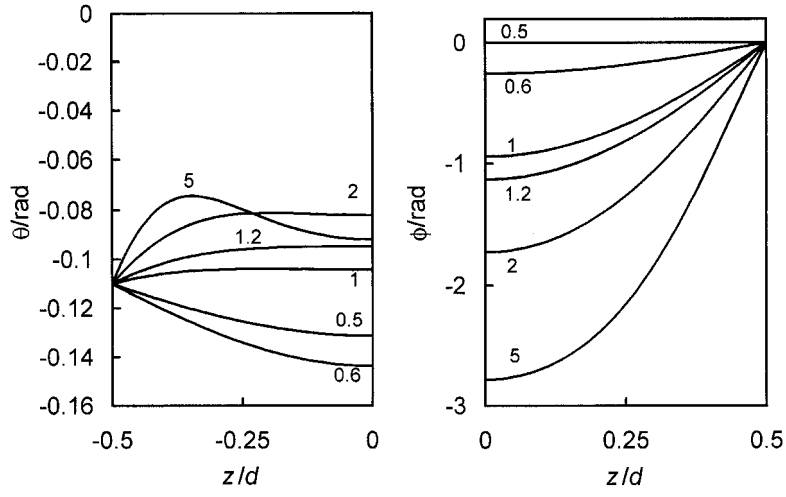

Figure 6. Director semi-profiles $\theta(z)$ [left] and $\phi(z)$ [right] for $\theta_s = -0{\cdot}11$ rad. The reduced shear stress values are indicated for each curve.

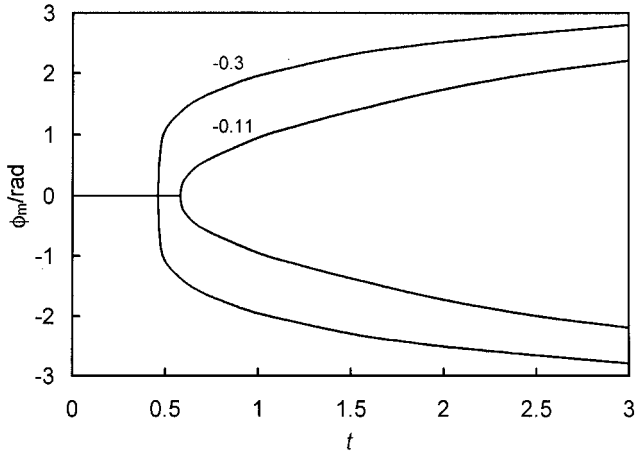

Figure 7. Mid-plane orientation angles ϕ_m as functions of shear stress t for two surface orientations, $\theta_s = -0{\cdot}11$ and $-0{\cdot}3$ rad. Both signs of the deviation angles are equivalent due to mirror symmetry with respect to the shear plane.

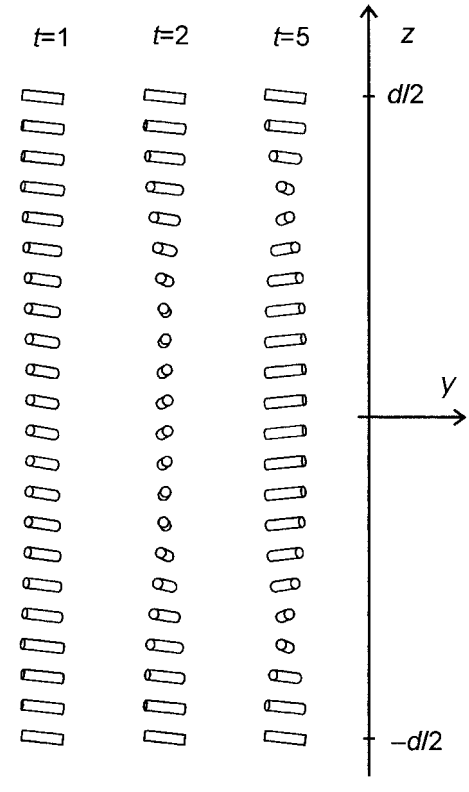

Figure 8. Structures of the deformed layer at three shear stress values, $\theta_s = -0{\cdot}11$ rad.

ment angle. The transverse velocities are about two orders of magnitude smaller than the longitudinal.

4. Discussion

In this paper, one-dimensional deformations of the sheared nematic layer have been studied numerically. The previously predicted director deviation from the plane of shear was confirmed. The director profiles $\theta(z)$ and $\phi(z)$ were calculated for various shear stresses and surface orientations; the transverse shear stress, effective viscosity, and longitudinal and transverse velocity profiles $v_y(z)$ and $v_x(z)$ were found.

The director emerging from the shear plane was predicted earlier from qualitative considerations based on catastrophe theory [4]. The threshold character of this effect was revealed and the formula for the threshold stress was given. It was found that the configuration in which the director lay in the plane of shear lost its stability under increasing shear stress. Equilibrium states above the threshold had not been determined in ref. [4] due to the limitations of the approach applied.

In the present paper we have found such states numerically. Their stability can be studied by means of

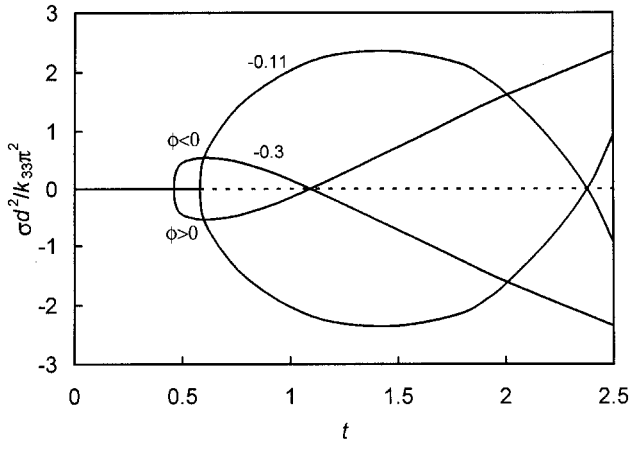

Figure 9. Transverse shear stresses σ as functions of t for two oblique orientations, $\theta_s = -0{\cdot}11$ and $\theta_s = -0{\cdot}3$ rad. Two branches for each θ_s value correspond to two signs of the deviation angles ϕ.

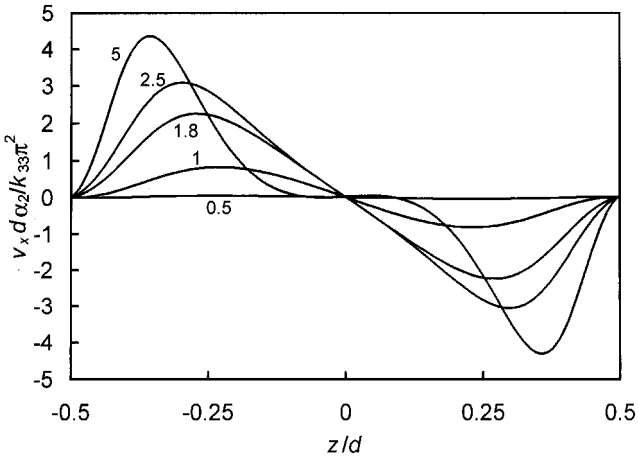

Figure 12. Transverse velocity profiles $v_x(z)$ for $\theta_s = -0{\cdot}3$ rad. The reduced shear stress values are indicated for each curve.

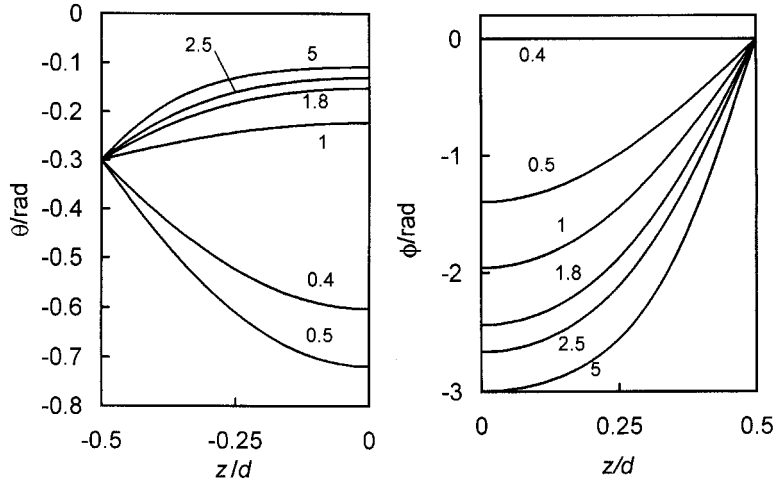

Figure 10. Director semi-profiles $\theta(z)$ [left] and $\phi(z)$ [right] for $\theta_s = -0{\cdot}3$ rad. The reduced shear stress values are indicated for each curve.

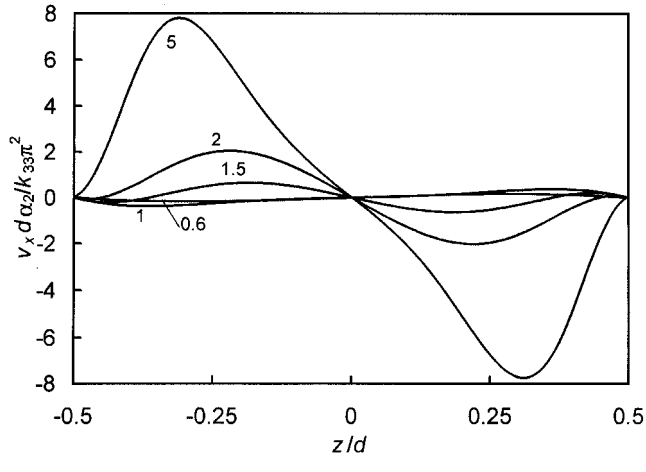

Figure 11. Transverse velocity profiles $v_x(z)$ for $\theta_s = -0{\cdot}11$ rad. The reduced shear stress values are indicated for each curve.

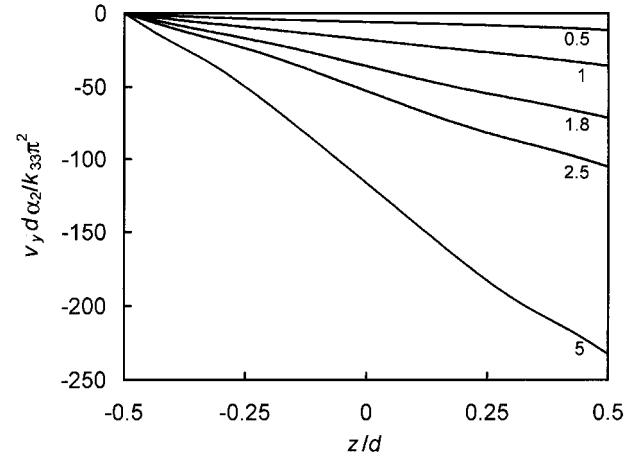

Figure 13. Longitudinal velocity profiles $v_y(z)$ for $\theta_s = -0{\cdot}3$ rad. The reduced shear stress values are indicated for each curve.

analysis of the total free energy per unit area of the layer, related to the director distributions for which $\phi(z) \neq 0$. For this purpose we have described approximately the deviation from the shear plane by the trial function $\phi(z) = \phi_0 \cos(\pi z/d)$. For the sake of simplicity, the surface orientation $\theta_s = -\theta_c$ was chosen, since it gives the known equilibrium uniform configuration at any shear stress [3, 4]. Under this condition, the deformation takes a form of pure rotation about the z axis and the free energy density g can be calculated as

$$g = \int_0^{\phi} \Gamma_z \, d\phi \tag{17}$$

where Γ_z is the z component of the total torque density [4]. The total free energy

$$G = \int_{-d/2}^{d/2} g \, dz \tag{18}$$

depends only on the single variable ϕ_0. We performed the integrations in equations (17) and (18) numerically for various ϕ_0 and t, leading to a set of $G(\phi_0)$ functions for several shear stresses (figure 14). This set of functions illustrates the behaviour which is characteristic for systems described by the cusp catastrophe [5]. Bifurcation of the stable states evident for this case corresponds to our results presented in figure 7. Therefore we are convinced that the deformed states which we have found are stable and that there are no other stable states, at least in the vicinity of the threshold. The study of the function $G(\phi_0)$ allowed determination of the threshold shear stress, $t_c = 0{\cdot}77$. This value coincides with results which were obtained by the torques balance method applied for $\theta_s = -0{\cdot}997$ and which are shown in figure 15. The value calculated by use of the formula

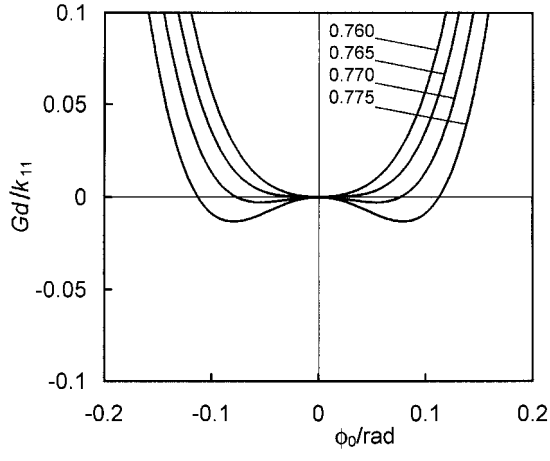

Figure 14. Total free energy of the deformed layer for various shear stresses as a function of deviation amplitude ϕ_0. The reduced shear stress values are indicated for each curve.

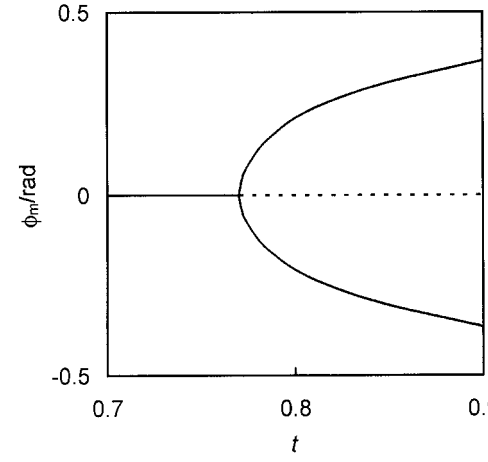

Figure 15. Bifurcation of the equilibrium states of the deformed layer. The dotted line denotes unstable equilibrium states.

derived in ref. [4] is 0·815; this small discrepancy is probably due to the simplifications made in ref. [4].

For reasonable parameters of the sample ($d = 10 \rightarrow 100\,\mu m$, $k_{33} = 10^{-11}$ N), the reduced threshold shear stress t of the order of 1 yields $\tau_{threshold} \approx 1 \rightarrow 10^{-2}$ N m^{-2}, which corresponds to the velocity of the upper plate $V = V_{threshold} = 10^{-3} \rightarrow 10^{-4}$ m s^{-1}, respectively. Experimental evidence of the director rotation out of the shear plane can be troublesome to achieve. First, a suitable surface orientation angle θ_s is necessary; then the use of conoscopic observations is required to determine the director rotation [6]. Measurement of the effective viscosity coefficient as a function of t in the vicinity of the threshold could serve as an alternative way of detection of the deviation from the shear plane. Our calculations were restricted to defect-free deformations, but production of disclination loops disturbing the flow alignment can be expected [6, 7].

The one-dimensional deformations considered in this paper are adequate for the infinite layer. We believe, that the results obtained here approximate properly to the behaviour of a liquid crystal in real finite layer, since the transverse velocities are about two orders of magnitude smaller than the longitudinal. One may expect that their influence on the director distribution is negligible. The transverse effects can be ignored and the results obtained here can be treated as adequate for experiments in which the lateral layer boundaries prevent transverse flow.

Summarizing, emergence from the shear plane should not be treated as a separate effect appearing during the flow, but rather as a way in which the usual flow-aligned structure is approached. This way is realized when suitable boundary conditions are imposed and when a relatively small twist elastic constant makes it preferable.

Appendix

Detailed form of the governing equations

Our aim was to find the stationary director distribution realized under the action of longitudinal shear stress τ. In this equilibrium state, the total torque acting on the director should vanish at every point of the layer. We approximated the real director distribution by the angles θ^i and ϕ^i assigned to each of the N sub-layers. Starting from some initial values of these angles, we were able to calculate the total torque Γ^i per unit volume in the ith sub-layer. In order to achieve the zero torque structure, the sum of the absolute values $|\Gamma^i|$ was decreased by sequentially varying θ^i and ϕ^i during the iterative process. The set of θ^i and ϕ^i which gave a sufficiently low sum, $\Sigma_{i=1}^{N}|\Gamma^i|$, was taken as the equilibrium state sought.

The torques for the ith inner sub-layer are given by

$$\Gamma^i=\Gamma^i_{\text{elastic}}+\Gamma^i_{\text{viscous}} \qquad \text{for } 1<i<N \tag{A1}$$

and for the boundary sub-layers by

$$\Gamma^1=\Gamma^1_{\text{elastic}}+\Gamma^1_{\text{viscous}}+\Gamma^1_{\text{anchoring}} \tag{A2}$$

$$\Gamma^N=\Gamma^N_{\text{elastic}}+\Gamma^N_{\text{viscous}}+\Gamma^N_{\text{anchoring}}. \tag{A3}$$

The elastic torques given by equations (3) and (4) were expressed by

$$\Gamma^i_{\text{elastic}}=\mathbf{n}^i\times\mathbf{h}^i. \tag{A4}$$

The components of $\mathbf{n}^i$ and $\mathbf{h}^i$ were as follows

$$n^i_x=\cos\theta^i\sin\phi^i \tag{A5}$$

$$n^i_y=\cos\theta^i\cos\phi^i \tag{A6}$$

$$n^i_z=\sin\theta^i \tag{A7}$$

$$\begin{aligned}h^i_x=&-2k_t n^i_y n^i_{x,z}n^i_{y,z}+(2k_t-k_b)n^i_x n^{i2}_{y,z}-k_t n^{i2}_y n^i_{x,zz}\\&+(k_t-k_b)n^i_x n^i_y n^i_{y,zz}-2k_b n^i_z n^i_{x,z}n^i_{z,z}\\&-k_b(n^{i2}_x+n^{i2}_z)n^i_{x,zz}-k_b n^i_x n^{i2}_{x,z}\end{aligned} \tag{A8}$$

$$\begin{aligned}h^i_y=&-2k_t n^i_x n^i_{x,z}n^i_{y,z}+(2k_t-k_b)n^i_y n^{i2}_{x,z}-k_t n^{i2}_x n^i_{y,zz}\\&+(k_t-k_b)n^i_x n^i_y n^i_{x,zz}-2k_b n^i_z n^i_{y,z}n^i_{z,z}\\&-k_b(n^{i2}_y+n^{i2}_z)n^i_{y,zz}-k_b n^i_y n^{i2}_{y,z}\end{aligned} \tag{A9}$$

$$h^i_z=k_b(n^{i2}_{x,z}+n^{i2}_{y,z})n^i_z-n^i_{z,zz} \tag{A10}$$

where $n^i_{j,k}$ and $n^i_{j,kl}$ denote the spatial derivatives of the director components.

The viscous torque for the ith sub-layer was calculated by means of equation (5) rewritten in the form

$$\Gamma^i_{\text{viscous}}=\mathbf{n}^i\times\mathbf{f}'^i. \tag{A11}$$

The components of $\mathbf{f}'^i$ were expressed in dimensionless form

$$f'^i_x=w^i n^i_z \tag{A12}$$

$$f'^i_y=u^i n^i_z \tag{A13}$$

$$f'^i_z=a_3(u^i n^i_y+w^i n^i_x) \tag{A14}$$

where $u^i=\partial v^i_y/\partial z$ and $w^i=\partial v^i_x/\partial z$, and $a_3=\alpha_3/\alpha_2$. The velocity gradients u^i and w^i for each sub-layer were calculated by solving the set of equations (7) written in dimensionless form

$$\left.\begin{aligned}t&=u^i p^i+w^i q^i\\ s&=u^i q^i+w^i r^i\end{aligned}\right\} \tag{A15}$$

where

$$p^i=\frac{1}{2}[2a_1 n^{i2}_y n^{i2}_z+(a_5-1)n^{i2}_z+(a_3+a_6)n^{i2}_y+a_4] \tag{A16}$$

$$q^i=\frac{1}{2}[2a_1 n^i_x n^i_y n^{i2}_z+(a_3+a_6)n^i_x n^i_y] \tag{A17}$$

$$r^i=\frac{1}{2}[2a_1 n^{i2}_x n^{i2}_z+(a_5-a_2)n^{i2}_z+(a_3+a_6)n^{i2}_x+a_4] \tag{A18}$$

and $a_k=\alpha_k/\alpha_2$. The dimensionless form s of the transverse stress σ was obtained by numerical integration [equation (12)]

$$s=\frac{\sum_{i=1}^{N-1}\left(\dfrac{q^i}{\delta^i}+\dfrac{q^{i+1}}{\delta^{i+1}}\right)}{\sum_{i=1}^{N-1}\left(\dfrac{p^i}{\delta^i}+\dfrac{p^{i+1}}{\delta^{i+1}}\right)} \tag{A19}$$

where $\delta^i=p^i r^i-q^{i2}$.

The boundary conditions were chosen to be identical on both plates. Therefore, the surface torques, calculated for the two sub-layers adjacent to the boundary plates and referred to unit volume, were expressed by

$$\Gamma^i_{\text{anchoring}}=2\frac{W d}{k_{11}}(N-1)(\mathbf{n}^i\ \mathbf{e}^i)(\mathbf{n}^i\times\mathbf{e}^i), \qquad i=1 \text{ or } N \tag{A20}$$

where the easy axis versors had the components

$$e^i_x=\cos\theta^i_s\sin\phi^i_s \tag{A21}$$

$$e^i_y=\cos\theta^i_s\cos\phi^i_s \tag{A22}$$

$$e^i_z=\sin\theta^i_s. \tag{A23}$$

References

[1] Leslie, F. M., 1979, *Adv. liq. Cryst.*, **4,** 1.

[2] Macsithigh, G. P., and Currie, P. K., 1977, *J. Phys. D*, **10,** 1471.

[3] Derfel, G., 1989, *Liq. Cryst.*, **6,** 709.

[4] Derfel, G., 1991, *Liq. Cryst.*, **10,** 647.

[5] Poston, T., and Stewart, I., 1976, *Taylor Expansions and Catastrophes* (Pitman).

[6] Mather, P. T., Pearson, D. S., and Larson, R. G., 1996, *Liq. Cryst.*, **20,** 539.

[7] Mather, P. T., Pearson, D. S., and Larson, R. G., 1996, *Liq. Cryst.*, **20,** 527.